

Locally anisotropic covariance functions on the sphere

Jian Cao* Jingjie Zhang* Zhuoer Sun* Matthias Katzfuss*[†]

Abstract

Rapid developments in satellite remote-sensing technology have enabled the collection of geospatial data on a global scale, hence increasing the need for covariance functions that can capture spatial dependence on spherical domains. We propose a general method of constructing nonstationary, locally anisotropic covariance functions on the sphere based on covariance functions in \mathbb{R}^3 . We also provide theorems that specify the conditions under which the resulting correlation function is isotropic or axially symmetric. For large datasets on the sphere commonly seen in modern applications, the Vecchia approximation is used to achieve higher scalability on statistical inference. The importance of flexible covariance structures is demonstrated numerically using simulated data and a precipitation dataset.

Keywords: axial symmetry; local anisotropy; nonstationarity; global data; Vecchia approximation

1 Introduction

Traditionally, geostatistical analysis relied on approximating small or regional spatial domains as flat subsets of \mathbb{R}^2 . However, since the deployment of satellites in the collection of global data, there is an increasing demand for covariance functions that are valid on spheres. In this paper, we aim to propose a new family of spherical covariance functions, defined over the unit 2-sphere $\mathbb{S} = \{\tilde{\mathbf{s}} \in \mathbb{R}^3 : \|\tilde{\mathbf{s}}\| = 1\}$, which are able to capture non-stationary features commonly observed in geostatistical datasets.

For processes defined over \mathbb{S} , two different distance measures are commonly used, namely the great-arc (or great-circle) distance, which measures the distance “going along the surface of the sphere”, and the Euclidean or chordal distance that “pierces through the sphere.” The relationship between great-arc distance and chordal distance on \mathbb{S} is given by:

$$r = 2 \sin(\theta/2), \tag{1}$$

where r is the chordal distance between two points on \mathbb{S} , and θ is the corresponding great-arc distance. Although a function of chordal distance is naturally a function of great-circle distance, finding a valid correlation function directly based on great-arc distance is not trivial

*Department of Statistics, Texas A&M University

[†]Corresponding author: katzfuss@gmail.com

(e.g., Jones, 1963) due to the curvature of \mathbb{S} . Most well-known covariance functions are valid (i.e., positive definite) on \mathbb{R}^d , for $d \geq 1$, only under Euclidean or Mahalanobis distance, yet may become invalid under great-arc distance (e.g., Gneiting, 2013). For example, the Matérn covariance function is only valid under great-arc distance if its smoothness is no greater than 0.5 (Gneiting, 2013).

Huang et al. (2011) summarized the validity of commonly used covariance functions under great-arc distance, most of which focused on isotropic covariance functions. Gneiting (2013) further developed characterizations and constructions of isotropic positive definite functions on spheres, and proved that subject to a natural support condition, many isotropic positive-definite functions on the Euclidean space \mathbb{R}^3 allow for the direct substitution of the chordal distance by the great-arc distance on the sphere. Ma (2012, 2015) constructed a family of isotropic covariance functions with polynomials. Similarly, Du et al. (2013) designed isotropic variogram functions on spheres using an infinite sum of the products of positive definite matrices and ultraspherical polynomials. Alegría et al. (2021) proposed the \mathcal{F} family of isotropic covariance functions that parameterizes the differentiability of the Gaussian field, which was shown to outperform the Matérn covariance function using chordal distance.

Popular approaches to modeling nonstationary or anisotropic processes on the sphere are reviewed in Jeong et al. (2017), including the differential operators (Jun and Stein, 2007, 2008; Jun, 2014), spherical harmonic representations (Stein et al., 2007), stochastic partial differential equations (Lindgren et al., 2011), kernel convolutions (Heaton et al., 2014), and multi-step spectrum methods (Castruccio et al., 2013; Castruccio and Genton, 2014, 2016). Hitzenko and Stein (2012) investigated the theoretical properties of a class of anisotropic processes on the sphere from applying first-order differential operators to an isotropic process. Blake et al. (2022) proposed adaptations of three existing families of stationary spherical covariance functions, namely the construction from Stieltjes functions (Menegatto, 2020), the \mathcal{F} family (Alegría et al., 2021), and the spectral adaptive approach (Emery et al., 2021), to obtain nonstationarity. The above approaches typically require intricate design to be positive-definite and differentiable and are less intuitive for practitioners compared with the straight-forward covariance construction in \mathbb{R}^3 using the Euclidean distance.

Here, we follow the idea of Yaglom (1987), restricting a valid covariance function in \mathbb{R}^3 to \mathbb{S} under the chordal distance, which is guaranteed to be valid. Guinness and Fuentes (2016) showed that results from using chordal and great-arc distances are often indistinguishable. This makes intuitive sense, in that when two points on the sphere will tend to be (almost) uncorrelated when they are far apart and will have approximately equal chordal distance and great-arc distance (i.e., $\sin(\theta/2) \approx \theta/2$) when they are close.

Motivated by this observation, we propose a family of nonstationary, locally anisotropic covariance functions on the sphere based on the locally anisotropic covariance functions for Euclidean space proposed in Paciorek and Schervish (2006). Similar ideas were also discussed in Katzfuss (2011) and Knapp (2012). We will introduce the properties of our general covariance parameterization and specific parameterizations that lead to isotropic or axially symmetric covariance structures to suit various geostatistical applications. For large datasets on the sphere (e.g., with more than 10^4 points), straightforward computation of the Gaussian log-likelihood is too expensive for statistical inference, for which we use the Vecchia approximation (Vecchia, 1988) of Gaussian processes (GPs) in our numerical studies.

The remainder of this article is organized as follows. Section 2 reviews a nonstationary

correlation function on \mathbb{R}^d . In Section 3, we construct classes of nonstationary covariance functions on the sphere, and provide theorems that specify the conditions for isotropic and axially symmetric covariance structures. Section 4 reviews the Vecchia approximation for large spatial datasets. In Sections 5 and 6, we use simulated data and a precipitation dataset from a physical model to highlight the advantage of our flexible nonstationary covariance structure. Section 7 concludes. Proofs are provided in the Appendix. Code can be found at <https://github.com/katzfuss-group/sphere-local-aniso-cov/>.

2 Locally anisotropic covariance functions

In this section, we briefly review an intuitive construction for nonstationarity proposed in Paciorek and Schervish (2006) based on any isotropic correlation function, denoted by ρ , in \mathbb{R}^d for all $d \in \mathbb{N}$. Specifically, the nonstationary correlation function is composed as:

$$\rho_{NS}(\mathbf{s}_i, \mathbf{s}_j) = c(\mathbf{s}_i, \mathbf{s}_j)\rho(q(\mathbf{s}_i, \mathbf{s}_j)), \quad (2)$$

$$q(\mathbf{s}_i, \mathbf{s}_j) = \{2(\mathbf{s}_i - \mathbf{s}_j)'(\boldsymbol{\Sigma}(\mathbf{s}_i) + \boldsymbol{\Sigma}(\mathbf{s}_j))^{-1}(\mathbf{s}_i - \mathbf{s}_j)\}^{1/2}, \quad (3)$$

$$c(\mathbf{s}_i, \mathbf{s}_j) = |\boldsymbol{\Sigma}(\mathbf{s}_i)|^{1/4}|\boldsymbol{\Sigma}(\mathbf{s}_j)|^{1/4}|(\boldsymbol{\Sigma}(\mathbf{s}_i) + \boldsymbol{\Sigma}(\mathbf{s}_j))/2|^{-1/2}, \quad (4)$$

where the positive-definite $d \times d$ matrix $\boldsymbol{\Sigma}(\mathbf{s}_i)$ is the local anisotropy matrix describing the spatially varying rotation and scaling, $q(\mathbf{s}_i, \mathbf{s}_j)$ is the Mahalanobis distance with respect to the average anisotropy matrix $(\boldsymbol{\Sigma}(\mathbf{s}_i) + \boldsymbol{\Sigma}(\mathbf{s}_j))/2$, and $c(\mathbf{s}_i, \mathbf{s}_j)$ is the normalization term. The anisotropy matrix $\boldsymbol{\Sigma}(\mathbf{s})$ at each location needs to be positive definite matrices in $\mathbb{R}^{d \times d}$, to which we assign the local rotational and scaling effects at the location \mathbf{s} . Hence, spatially-varying anisotropy is achieved in the covariance structure represented by Equations (2), (3), and (4).

This nonstationarity design combines different local anisotropic correlation structures into a valid global correlation function, leading to greater model expressiveness. Under the assumption that the anisotropy matrix $\boldsymbol{\Sigma}(\mathbf{s})$ varies smoothly across the domain, the differentiability of ρ_{NS} follows that of the underlying stationary covariance function ρ (Paciorek and Schervish, 2006). When ρ is chosen as the isotropic Matérn covariance function, one may also vary the smoothness parameter across the domain to achieve different local smoothness; see Section 3.3 for a detailed description.

3 Classes of nonstationary covariance functions on the sphere

Given the intuitive construction for nonstationarity in Section 2, an important question is how to parameterize the anisotropy matrix $\boldsymbol{\Sigma}(\mathbf{s})$ to better capture the local covariance structure, which can be largely problem dependent. In this section, we consider one general parameterization of $\boldsymbol{\Sigma}(\mathbf{s})$ that represents local rotation and scaling on a tangent plane of the sphere and probe the conditions for achieving the special cases of isotropic and axially symmetric covariance functions.

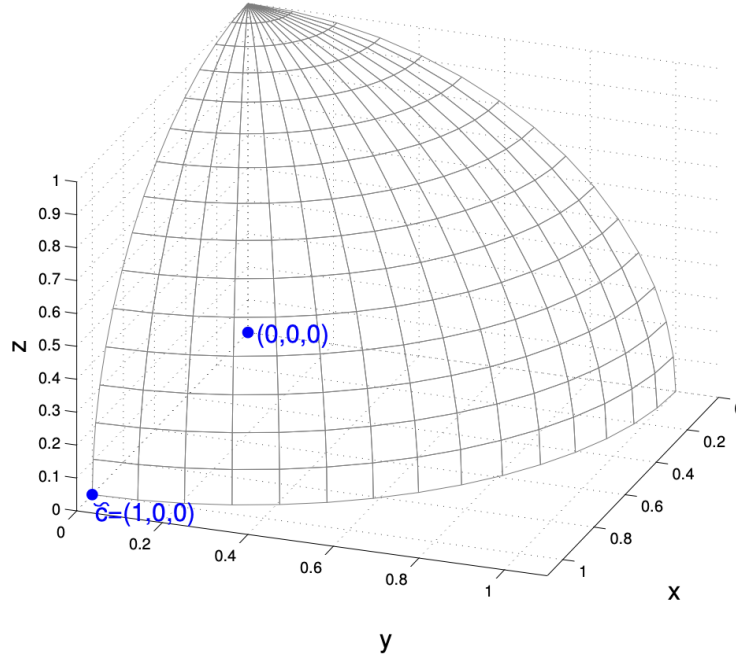


Figure 1: The part of a unit sphere centered at the origin that lies in the first octant of the Cartesian coordinate system, where all coordinates are positive. The origin and the point \mathbf{c} referred to in the text are shown in blue.

3.1 Construction of the covariance functions

Without loss of generality, assume that \mathbb{S} is centered at the origin in \mathbb{R}^3 , $(0, 0, 0)$, and that the intersection of the prime meridian and the equator, denoted by $\mathbf{c} := (0, 0)$ (0° longitude, 0° latitude), is located on the x -axis (i.e., it has the Euclidean coordinates $\tilde{\mathbf{c}} := (1, 0, 0)$). Figure 1 shows the part of the sphere that lies in the first (positive) octant of a Cartesian coordinate system, including the origin and \mathbf{c} . The Euclidean coordinates $\tilde{\mathbf{s}} = (x, y, z)$ of any point $\mathbf{s} = (l, L)$ with longitude l and latitude L on \mathbb{S} are given by:

$$x = \cos(L) \cos(l), \quad y = \cos(L) \sin(l), \quad z = \sin(L).$$

For d -dimensional Euclidean space, we can parameterize $\Sigma(\mathbf{s})$ using d scaling parameters and $d - 1$ rotation parameters (see, e.g., Banerjee et al., 2008). Although \mathbb{S} “lives” in \mathbb{R}^3 , the surface of \mathbb{S} is (locally) a two-dimensional space (i.e., the tangent plane) at any point $\mathbf{s} \in \mathbb{S}$, indicating a parameterization with only two local scaling and one local rotation parameters. Consider the tangent plane at \mathbf{c} , which is the (y, z) -plane, as shown in Figure 1. We use $\gamma_1(\mathbf{c}) > 0$ and $\gamma_2(\mathbf{c}) > 0$ as the scaling parameters in the y and z -directions, respectively, and $\kappa(\mathbf{c}) \in [0, \pi/2)$ as the rotation parameter, whose collective effect is shown in Figure 2. Specifically, the scaling matrix at \mathbf{c} is a diagonal matrix $\mathbf{D}(\boldsymbol{\gamma}) := \text{diag}\{1, \gamma_1, \gamma_2\}$ and the rotation matrix that rotates the (y, z) -plane at $\tilde{\mathbf{c}}$ about the x -axis is given by:

$$\mathcal{R}_x(\kappa) := \begin{pmatrix} 1 & 0 & 0 \\ 0 & \cos \kappa & -\sin \kappa \\ 0 & \sin \kappa & \cos \kappa \end{pmatrix}.$$

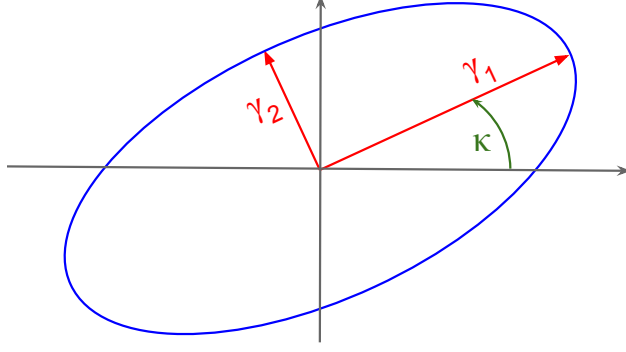


Figure 2: Illustration of the scaling parameters γ_1 and γ_2 and the rotation parameter κ at reference point $\tilde{\mathbf{c}}$, along with an oval representing the resulting correlation contour

The anisotropy matrix at the reference point $\tilde{\mathbf{c}}$ (spherical coordinates \mathbf{c}) is then given by:

$$\tilde{\Sigma}(\mathbf{c}) := \mathcal{R}_x(\kappa(\mathbf{c}))\mathbf{D}(\boldsymbol{\gamma}(\mathbf{c}))\mathcal{R}_x(\kappa(\mathbf{c}))'. \quad (5)$$

Consider an arbitrary location \mathbf{s} on the \mathbb{S} , whose Euclidean coordinates are denoted by $\tilde{\mathbf{s}}$. The way we construct the anisotropy matrix for \mathbf{s} , denoted by $\Sigma(\mathbf{s})$, is to left- and right-multiply (5) by the rotation matrix $\mathcal{R}(\mathbf{s})$ such that $\tilde{\mathbf{s}}'\Sigma(\mathbf{s})^{-1}\tilde{\mathbf{s}} = \tilde{\mathbf{s}}'(\mathcal{R}(\mathbf{s})\tilde{\Sigma}(\mathbf{s})\mathcal{R}(\mathbf{s})')^{-1}\tilde{\mathbf{s}} = \tilde{\mathbf{c}}'\tilde{\Sigma}(\mathbf{s})^{-1}\tilde{\mathbf{c}}$. Here, $\tilde{\Sigma}(\mathbf{s})$ is parameterized by $\kappa(\mathbf{s})$ and $\boldsymbol{\gamma}(\mathbf{s})$, similar to (5), denoting the local rotation and scaling at \mathbf{s} measured at the reference point \mathbf{c} . To rotate \mathbf{s} to \mathbf{c} , we can rotate $\tilde{\mathbf{s}}$ about the y -axis and z -axis by $-L$ and $-l$, respectively, which is equivalent to left-multiplication of $\tilde{\mathbf{c}}$ by $\mathcal{R}_y(-L)\mathcal{R}_z(-l)$, where

$$\mathcal{R}_y(\theta) := \begin{pmatrix} \cos \theta & 0 & \sin \theta \\ 0 & 1 & 0 \\ -\sin \theta & 0 & \cos \theta \end{pmatrix} \quad \text{and} \quad \mathcal{R}_z(\theta) := \begin{pmatrix} \cos \theta & -\sin \theta & 0 \\ \sin \theta & \cos \theta & 0 \\ 0 & 0 & 1 \end{pmatrix}.$$

Hence, $\mathcal{R}(\mathbf{s})$ and $\Sigma(\mathbf{s})$ are defined as $\mathcal{R}_z(l)\mathcal{R}_y(L)$ and $\mathcal{R}_z(l)\mathcal{R}_y(L)\tilde{\Sigma}(\mathbf{s})\mathcal{R}_y(L)'\mathcal{R}_z(l)'$, respectively. Therefore, at an arbitrary location \mathbf{s} , we have:

$$\tilde{\mathbf{s}}'\Sigma(\mathbf{s})^{-1}\tilde{\mathbf{s}} = \tilde{\mathbf{c}}'\tilde{\Sigma}(\mathbf{s})^{-1}\tilde{\mathbf{c}} = \tilde{\mathbf{c}}'\left(\mathcal{R}_x(\kappa(\mathbf{s}))\mathbf{D}(\boldsymbol{\gamma}(\mathbf{s}))\mathcal{R}_x(\kappa(\mathbf{s}))'\right)^{-1}\tilde{\mathbf{c}}.$$

The anisotropy matrix $\Sigma(\mathbf{s})$ achieves nonstationarity through introducing local rotation and scaling. One can further increase the nonstationarity through assuming heterogeneous variances in the domain $\sigma^2(\mathbf{s}) > 0$, with which the covariance function between two locations \mathbf{s}_i and \mathbf{s}_j amounts to:

$$C(\mathbf{s}_i, \mathbf{s}_j) = \sigma(\mathbf{s}_i)\sigma(\mathbf{s}_j)\rho_{NS}(\mathbf{s}_i, \mathbf{s}_j),$$

where $\rho_{NS}(\mathbf{s}_i, \mathbf{s}_j)$ is defined by (2) to (4) through the anisotropy matrix $\Sigma(\mathbf{s})$.

3.2 Properties

The approach above provides a parameterization of $\Sigma(\mathbf{s})$ in terms of two spatially varying ranges, $\boldsymbol{\gamma}(\mathbf{s})$, and one spatially varying rotation, $\kappa(\mathbf{s})$, which can in turn be parameterized

in suitable ways for different applications. In this section, we provide conditions on $\gamma(\mathbf{s})$ and $\kappa(\mathbf{s})$ such that the resulting correlation function in (2) is isotropic or axially symmetric; proofs of the theorems are included in Appendix A.

An isotropic covariance function is a function of only distance between two locations. Due to the one-to-one relationship between the great-arc and the chordal distances in (1), isotropic covariance functions on the sphere are isotropic with respect to both chordal and great-arc distance. By adding constraints to the scaling parameters $\gamma_1(\mathbf{s})$ and $\gamma_2(\mathbf{s})$, the correlation function ρ_{NS} in (2) can achieve isotropy on the sphere:

THEOREM 1. *The correlation function ρ_{NS} in (2) is isotropic (i.e., depends only on distance) if $\gamma_1(\mathbf{s}) = \gamma_2(\mathbf{s}) \equiv \gamma$ is constant.*

A subclass of covariance functions that are especially useful for spherical domains are axially symmetric covariance functions (e.g., Stein et al., 2007), under which the correlation between a pair of locations on the sphere depends on longitudes only through the longitude difference:

DEFINITION. *A covariance function $C : \mathbb{S} \times \mathbb{S} \rightarrow \mathbb{R}$ is called axially symmetric if there exists a function C_A such that*

$$C(\mathbf{s}_i, \mathbf{s}_j) = C_A(l_i - l_j, L_i, L_j),$$

where $\mathbf{s}_i = (l_i, L_i)$ and $\mathbf{s}_j = (l_j, L_j)$ with longitudes l_i and l_j and latitudes L_i and L_j on \mathbb{S} .

Axially symmetric covariance functions can be also obtained based on the Theorem below:

THEOREM 2. *The correlation function ρ_{NS} in (2) is axially symmetric if $\kappa(\mathbf{s}) \equiv 0$ and $\gamma_1(\cdot)$ and $\gamma_2(\cdot)$ are functions of latitude only (i.e., they do not depend on longitude).*

Special cases of our general nonstationary covariance function that include isotropic, anisotropic, axially symmetric, and general nonstationary parameterizations are visualized in Figure 3.

3.3 Example: A nonstationary Matérn covariance on the sphere

The Matérn correlation function is highly popular in geospatial analysis. It is valid in \mathbb{R}^d for any $d \in \mathbb{N}$ and given by

$$\mathcal{M}_\nu(r) = \frac{2^{1-\nu}}{\Gamma(\nu)} r^\nu \mathcal{K}_\nu(r), \quad r \geq 0,$$

where $\mathcal{K}_\nu(\cdot)$ is the modified Bessel function of order $\nu > 0$. The standard deviation, say $\sigma(\cdot)$, and the smoothness parameter $\nu(\cdot)$ in the Matérn can also vary over space (Stein, 2005). Hence, we can obtain a highly flexible Matérn covariance on the sphere of the form

$$\mathcal{M}_{NS}(\mathbf{s}_i, \mathbf{s}_j) = \sigma(\mathbf{s}_i)\sigma(\mathbf{s}_j)c(\mathbf{s}_i, \mathbf{s}_j)\mathcal{M}_{(\nu(\mathbf{s}_i)+\nu(\mathbf{s}_j))/2}(q(\mathbf{s}_i, \mathbf{s}_j)), \quad (6)$$

where c, q are as in (3)–(4), and $\Sigma(\mathbf{s})$ can be parameterized in terms of spatially varying scales $\gamma(\mathbf{s})$ and rotation $\rho(\mathbf{s})$ as in Section 3.1.

Guinness and Fuentes (2016) showed that the local smoothness properties of the Matérn covariance are preserved when restricting a process in Euclidean space to the sphere. Specifically, a GP with covariance function \mathcal{M}_{NS} has m mean square derivatives at \mathbf{s} if and only if $\nu(\mathbf{s}) > m$.

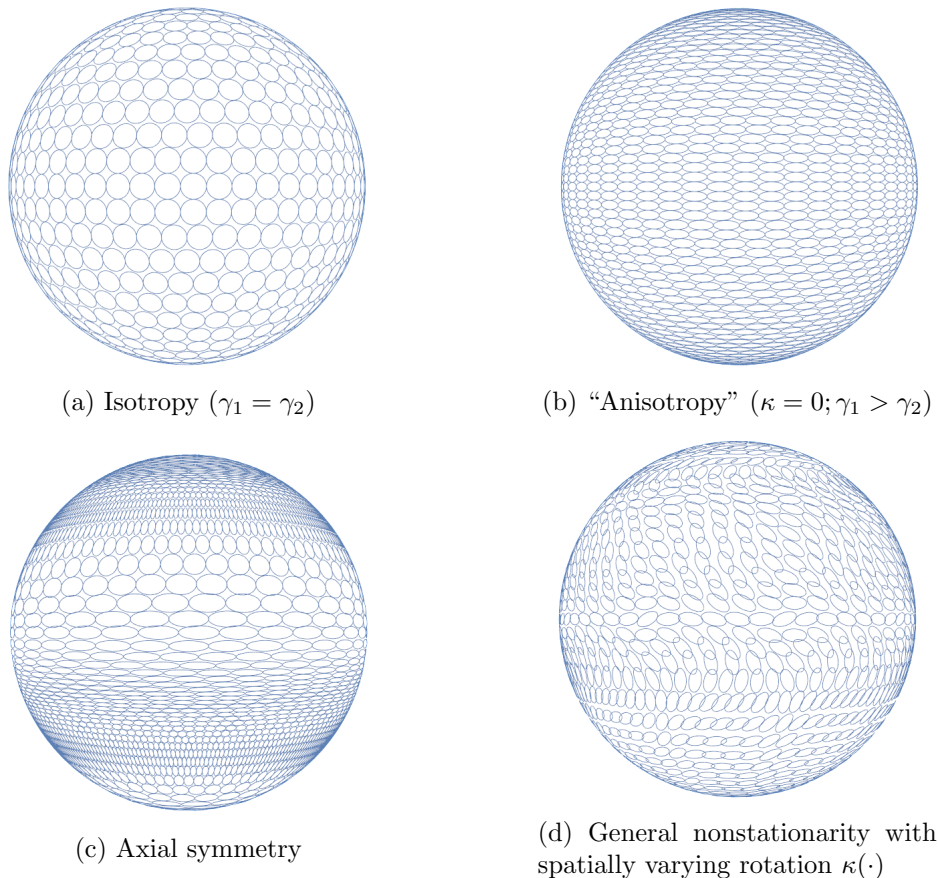


Figure 3: Illustration of special cases of the nonstationary correlation functions in (2) via correlation contours

4 Vecchia approximation

For many modern large datasets, including on the sphere, direct application of GPs is too computationally expensive, as the cost scales cubically in the number of data points. The approximation proposed by Vecchia (1988) has become highly popular in recent years, which has linear computational complexity and straight-forward parallel features while maintaining high accuracy measured by the KL divergence from the true process (e.g., Guinness, 2018; Katzfuss and Guinness, 2021). Based on a given ordering of the observations, the Vecchia approximation replaces the high-dimensional joint multivariate normal density with a product of univariate conditional normal densities, in which each variable conditions only on a small subset of previous observations in the ordering, amounting to an ordered conditionally independent approximation.

Denote $h(i) = \{1, 2, \dots, i - 1\}$ with $h(1) = \emptyset$ and $\mathbf{y}_{h(i)} = (y_1, \dots, y_{i-1})'$. Consider a GP $y(\cdot) \sim GP(0, C)$ on a spatial region \mathcal{D} with covariance function C . The distribution of the observation $\mathbf{y} = (y_1, y_2, \dots, y_n)$ is given by

$$f(\mathbf{y}) = \prod_{i=1}^n f(y_i | \mathbf{y}_{h(i)}).$$

The Vecchia approximation replaces $h(i)$ with a subset $g(i) \subset h(i)$, where $g(i)$ is usually

chosen to select those indices corresponding to the m observations nearest in distance to the i th observation. This leads to the following approximation of the joint density:

$$\hat{f}(\mathbf{y}) = \prod_{i=1}^n f(y_i | \mathbf{y}_{g(i)}). \quad (7)$$

The Vecchia approximation ensures computational feasibility for large spatial datasets. The choices for ordering the locations and selecting the conditioning sets $\{g(i)\}_{i=1}^n$ are typically based on distance or estimated correlation (Katzfuss and Guinness, 2021). Here, we will use maximum-minimum-distance ordering (Guinness, 2018) and nearest-neighbor conditioning in the numerical studies, both based on the Euclidean distances. Correlation-based ordering and conditioning that takes into account the potential nonstationary structure is also possible (Katzfuss et al., 2022; Kang and Katzfuss, 2021). Aside from likelihood-based parameter inference based on the Vecchia likelihood in (7), the Vecchia approximation can also be applied to unknown locations in order to obtain accurate approximations of posterior predictive distributions (e.g., Katzfuss et al., 2020a). In the case of noisy data, the Vecchia approximation can be applied to the latent (noise-free) GP as before, and then combined with an incomplete-Cholesky decomposition of the posterior precision matrix to preserve the low computational complexity (Schäfer et al., 2021). We implemented Vecchia inference based on our new covariance function by extending the R package `GPvecchia` (Katzfuss et al., 2020b).

5 Numerical study

We perform simulations to demonstrate the improvement of posterior inference gained from adopting a more flexible covariance structure. Specifically, we simulate GPs that are isotropic, axially symmetric, and generally nonstationary based on different parameterizations of the covariance structure introduced in (6). The scaling parameters $\gamma_1(\mathbf{s})$ and $\gamma_2(\mathbf{s})$ are parameterized as:

$$\gamma_1(\mathbf{s}) = \exp(\beta_{10} + \beta_{11} \sin(l) + \beta_{12} L), \quad (8)$$

$$\gamma_2(\mathbf{s}) = \exp(\beta_{20} + \beta_{21} \sin(l) + \beta_{22} L), \quad (9)$$

where $\mathbf{s} = (l, L)$ with longitude l and latitude L . Based on Theorems 1 and 2, isotropic, axially symmetric, and general nonstationary covariance structures are constructed as follows:

Isotropy: According to Theorem 1, the correlation function ρ_{NS} in (2) is isotropic if $\gamma_1(\mathbf{s}) = \gamma_2(\mathbf{s}) \equiv \gamma$ is constant, and so we set the parameters in (8)–(9) as

$$\beta_1 = (\beta_{10}, \beta_{11}, \beta_{12}) = (-0.5, 0, 0),$$

$$\beta_2 = (\beta_{20}, \beta_{21}, \beta_{22}) = (-0.5, 0, 0).$$

Axial symmetry: According to Theorem 2, the correlation function ρ_{NS} in (2) is axially symmetric if $\kappa(\mathbf{s}) \equiv 0$ and $\gamma_1(\cdot)$ and $\gamma_2(\cdot)$ are functions of latitude only and we set the parameters as

$$\beta_1 = (\beta_{10}, \beta_{11}, \beta_{12}) = (-0.5, 0, 1.44),$$

$$\beta_2 = (\beta_{20}, \beta_{21}, \beta_{22}) = (-3.2, 0, 1.44).$$

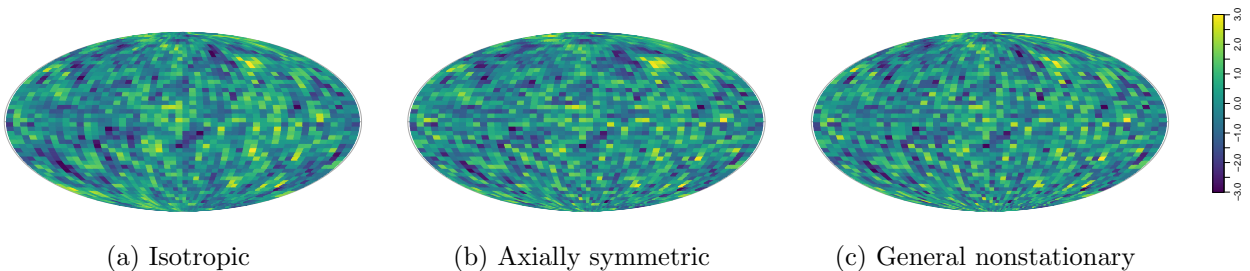


Figure 4: Realizations of the isotropic, axially symmetric, and general nonstationary GPs over a 50×50 grid on the sphere

General nonstationarity: A more general nonstationary covariance function can be obtained by setting

$$\begin{aligned} \kappa &= 0.8, \\ \beta_1 &= (\beta_{10}, \beta_{11}, \beta_{12}) = (-0.5, -1.2, 1.44), \\ \beta_2 &= (\beta_{20}, \beta_{21}, \beta_{22}) = (-3.2, -0.3, 1.44). \end{aligned}$$

Each dataset is generated on a regular latitude/longitude grid of size $50 \times 50 = 2,500$ on the sphere and then split into training and testing subsets, under two different scenarios: (a) a random sampling of 20% of all locations as the test dataset; (b) ten randomly selected regions, each with a longitudinal band width of 0.4 and a latitudinal band width of 0.2, that sum up to approximately 20% of all locations as the test dataset. The training dataset is then modeled by the three progressively more flexible covariance structures:

Isotropy: unknown β_{10}, β_{20} , with $\beta_{10} = \beta_{20}$ and fixed $\beta_{11} = \beta_{12} = \beta_{21} = \beta_{22} = \kappa = 0$.

Axial symmetry: unknown $\beta_{10}, \beta_{12}, \beta_{20}, \beta_{22}$, with fixed $\beta_{11} = \beta_{21} = \kappa = 0$.

General nonstationarity: unknown $\beta_{10}, \beta_{11}, \beta_{12}, \beta_{20}, \beta_{21}, \beta_{22}, \kappa$.

Realizations of the isotropic, axially symmetric, and general nonstationary GPs are shown in Figure 4. The prediction scores for the nine combinations of ‘true’ and ‘assumed’ covariance structures are summarized in Table 1 that include the mean absolute error (MAE), the root mean squared error (RMSE), the continuous ranked probability score (CRPS), and the energy score. MAE and RMSE consider only point predictions, CRPS evaluates marginal predictive distributions, and the energy score evaluates the joint predictive distribution for the entire test set. The variance and smoothness parameters of the Matérn covariance function $\mathcal{M}_\nu(r)$ are $\sigma(\mathbf{s}) = 1$ and $\nu(\mathbf{s}) = 0.5$, respectively, both considered as known. We ran an adaptive MCMC algorithm (Vihola, 2012) for 5,000 iterations for the Bayesian inference of unknown parameters. Within MCMC, the Vecchia approximation in (7) of the likelihood is applied, which uses the maximum-minimum-distance ordering and the nearest-neighbor conditioning with a conditioning set size of ten. To obtain the posterior predictive distribution at the testing locations, we also used the Vecchia approximation (i.e., ordinary kriging with ten nearest neighbors), based on MCMC samples of the unknown parameters after

(a) True model - Isotropic

	Random				Region			
	MAE	RMSE	CRPS	Energy	MAE	RMSE	CRPS	Energy
Isotropic	0.569	0.728	0.563	16.1	0.716	0.904	0.710	18.8
Axially symmetric	0.567	0.727	0.556	15.9	0.716	0.904	0.705	18.6
Nonstationary	0.568	0.728	0.551	15.7	0.716	0.904	0.698	18.4

(b) True model - Axially symmetric

	Random				Region			
	MAE	RMSE	CRPS	Energy	MAE	RMSE	CRPS	Energy
Isotropic	0.754	0.961	0.751	21.3	0.768	0.968	0.761	20.1
Axially symmetric	0.637	0.834	0.621	18.1	0.741	0.932	0.732	19.2
Nonstationary	0.637	0.835	0.616	18.0	0.741	0.931	0.727	19.1

(c) True model - Nonstationary

	Random				Region			
	MAE	RMSE	CRPS	Energy	MAE	RMSE	CRPS	Energy
Isotropic	0.734	0.938	0.730	20.8	0.777	0.973	0.773	20.3
Axially symmetric	0.688	0.883	0.671	19.2	0.761	0.953	0.752	19.6
Nonstationary	0.681	0.874	0.659	18.8	0.754	0.943	0.739	19.3

Table 1: Prediction scores (lower is better), each averaged over five simulated datasets, for the nine different combinations of the true and assumed covariance structures. Test sets are selected as random locations (Random) or regions (Region) that amount to 20% of the total dataset.

a burn-in of size one thousand; the resulting predictive distribution is a mixture of Gaussians. For datasets generated by isotropic GPs, the prediction scores are very close under the assumptions of isotropic, axially symmetric, and nonstationary covariance structures. The difference becomes more pronounced when the datasets are generated from an axially symmetric GP, where the axially symmetric and the nonstationary structures have similar performance, both significantly better than that of the isotropic covariance structure. Furthermore, in modeling the general nonstationary GPs, there is a uniform improvement in all prediction scores when switching from the axially symmetric covariance structure to the general nonstationary covariance structure. Hence, the prediction accuracy is barely affected when using a general flexible model when the true model is simple and the number of optimization parameters is small, but large gains are possible with a more flexible model when the true dependence structure is more complicated.

6 Application to real data

Using the same three types of covariance structures used in Section 5, we model a precipitation dataset from the Community Earth System Model (CESM) Large Ensemble Project

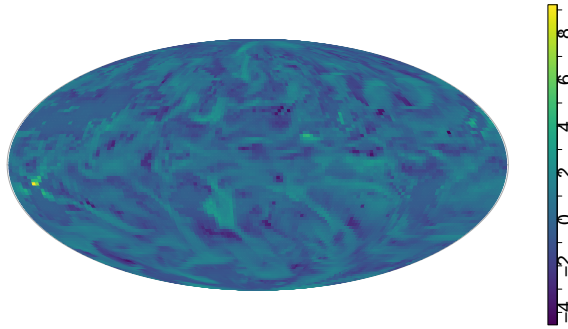


Figure 5: Visualization of the precipitation dataset after pre-processing

	Random				Region			
	MAE	RMSE	CRPS	Energy	MAE	RMSE	CRPS	Energy
Isotropic	0.383	0.549	0.376	27.1	0.756	0.967	0.749	43.1
Axially symmetric	0.268	0.426	0.264	21.6	0.654	0.834	0.649	37.7
Nonstationary	0.269	0.428	0.263	21.6	0.651	0.832	0.620	35.7

Table 2: Prediction scores, using the precipitation data, of isotropic, axially symmetric, and general non-stationary structures. Test sets are selected as random locations (Random) or regions (Region) that amount to 20% of the total dataset.

(Kay et al., 2015). After subsetting, the dataset contains precipitation rates (m/s) on July 1, 401, on a roughly a 2° resolution in terms of longitude and latitude, totaling $144 \times 96 = 13,824$ locations on a spherical grid. We consider the standardized log-precipitation anomalies shown in Figure 5, which does not indicate any distinct mean structure. 20% of the dataset is used for testing, selected either as random locations or as random regions, similar to Section 5.

Model parameters have the same initializations under the three model assumptions, and the smoothness parameter ν for the CESM dataset is fixed at 2.5 due to the increased smoothness compared with the simulated datasets in Figure 4. We also summarize the performance (e.g., scores) of posterior inference in Table 2. The isotropic covariance structure is significantly out-performed by the axially symmetric and the nonstationary structures while the difference between the latter two is indistinguishable. This indicates that using an isotropic covariance structure can be insufficient for practical modeling and the benefit of having a parsimonious flexible structure is likely to outweigh that of substituting the Euclidean distance with the chordal distance, especially when scalable GP approximations (e.g., the Vecchia approximation) are applied.

7 Conclusions

We proposed a general approach for constructing nonstationary, locally anisotropic covariance functions on the sphere based on isotropic covariance functions in \mathbb{R}^3 . Special parameterizations of the nonstationary covariance function that amount to isotropic and axially symmetric covariance structures were also discussed. Axially symmetric covariance functions

are widely used in geospatial analysis of global data and their advantages over isotropic covariance structures were demonstrated with both simulated Gaussian random fields and a CESM dataset. The extra flexibility of our nonstationary parameterization also improved posterior inference compared with the axially symmetric structure, although the improvement was less significant. For large datasets on the sphere, straightforward computation of Gaussian probabilities is too computationally expensive, and so we used the Vecchia approximation to achieve faster parameter estimation and posterior inference.

Acknowledgments

MK and JC were partially supported by National Science Foundation (NSF) Grant DMS-1654083. MK was also partially supported by NSF Grant DMS-1521676.

A Proofs

Proof of Theorem 1. If $\gamma_1(\mathbf{s}) = \gamma_2(\mathbf{s}) \equiv \gamma$ is constant, then

$$\mathbf{D}(\gamma) = \begin{pmatrix} 1 & 0 & 0 \\ 0 & \gamma & 0 \\ 0 & 0 & \gamma \end{pmatrix},$$

$$\begin{aligned} \tilde{\Sigma}(\mathbf{s}) &= \mathcal{R}_x(\kappa(s))\mathbf{D}(\gamma)\mathcal{R}_x(\kappa(s))' \\ &= \begin{pmatrix} 1 & 0 & 0 \\ 0 & \cos \kappa(s) & -\sin \kappa(s) \\ 0 & \sin \kappa(s) & \cos \kappa(s) \end{pmatrix} \begin{pmatrix} 1 & 0 & 0 \\ 0 & \gamma & 0 \\ 0 & 0 & \gamma \end{pmatrix} \begin{pmatrix} 1 & 0 & 0 \\ 0 & \cos \kappa(s) & \sin \kappa(s) \\ 0 & -\sin \kappa(s) & \cos \kappa(s) \end{pmatrix} \\ &= \begin{pmatrix} 1 & 0 & 0 \\ 0 & \gamma & 0 \\ 0 & 0 & \gamma \end{pmatrix}. \end{aligned}$$

To compute $\Sigma(\mathbf{s}) = \mathcal{R}_z(l)\mathcal{R}_y(L)\tilde{\Sigma}(\mathbf{s})\mathcal{R}_y(L)'\mathcal{R}_z(l)'$, we first compute

$$\begin{aligned} \mathbf{A} := \mathcal{R}_z(l)\mathcal{R}_y(L) &= \begin{pmatrix} \cos(l) & -\sin(l) & 0 \\ \sin(l) & \cos(l) & 0 \\ 0 & 0 & 1 \end{pmatrix} \begin{pmatrix} \cos(L) & 0 & \sin(L) \\ 0 & 1 & 0 \\ -\sin(L) & 0 & \cos(L) \end{pmatrix} \\ &= \begin{pmatrix} \cos(l)\cos(L) & -\sin(l)\cos(L) & \cos(l)\sin(L) \\ \sin(l)\cos(L) & \cos(l)\cos(L) & \sin(l)\sin(L) \\ -\sin(L) & 0 & \cos(L) \end{pmatrix}, \end{aligned}$$

$$\begin{aligned} \Sigma(\mathbf{s}) = \mathbf{A}\tilde{\Sigma}(\mathbf{s})\mathbf{A}' &= \begin{pmatrix} (1-\gamma)x^2 + \gamma & (1-\gamma)xy & (1-\gamma)xz \\ (1-\gamma)xy & (1-\gamma)y^2 + \gamma & (1-\gamma)yz \\ (1-\gamma)xz & (1-\gamma)yz & (1-\gamma)z^2 + \gamma \end{pmatrix} \\ &= (1-\gamma) \begin{pmatrix} x \\ y \\ z \end{pmatrix} \begin{pmatrix} x & y & z \end{pmatrix} + \gamma \mathbf{I}_3 \\ &= (1-\gamma)\tilde{\mathbf{s}}\tilde{\mathbf{s}}' + \gamma \mathbf{I}_3, \end{aligned}$$

where $x = \cos(L)\cos(l)$, $y = \cos(L)\sin(l)$, $z = \sin(L)$ are the (x, y, z) -coordinates of a 3-dimensional Cartesian coordinate system. Then

$$\begin{aligned}
|\Sigma(\mathbf{s})| &= \det\{(1-\gamma)\tilde{\mathbf{s}}\tilde{\mathbf{s}}' + \gamma\mathbf{I}_3\} \\
&= \gamma^3 \cdot \det\left\{\mathbf{I}_3 + \frac{1-\gamma}{\gamma}\tilde{\mathbf{s}}\tilde{\mathbf{s}}'\right\} \\
&= \gamma^3 \cdot \det\left\{1 + \frac{1-\gamma}{\gamma}\tilde{\mathbf{s}}'\tilde{\mathbf{s}}\right\} \\
&= \gamma^3 \cdot \det\left\{1 + \frac{1-\gamma}{\gamma} \cdot 1\right\} \\
&= \gamma^2
\end{aligned}$$

does not depend on \mathbf{s} . And for $i \neq j$,

$$(\Sigma(\mathbf{s}_i) + \Sigma(\mathbf{s}_j))^{-1} = ((1-\gamma)\tilde{\mathbf{s}}_i\tilde{\mathbf{s}}_i' + (1-\gamma)\tilde{\mathbf{s}}_j\tilde{\mathbf{s}}_j' + 2\gamma\mathbf{I}_3)^{-1}.$$

WLOG, we ignore the constant coefficients inside the inverse, and then

$$\begin{aligned}
(\Sigma(\mathbf{s}_i) + \Sigma(\mathbf{s}_j))^{-1} &= (\tilde{\mathbf{s}}_i\tilde{\mathbf{s}}_i' + \tilde{\mathbf{s}}_j\tilde{\mathbf{s}}_j' + \mathbf{I}_3)^{-1} \\
&= (\tilde{\mathbf{s}}_j\tilde{\mathbf{s}}_j' + \mathbf{I}_3)^{-1} - (\tilde{\mathbf{s}}_j\tilde{\mathbf{s}}_j' + \mathbf{I}_3)^{-1}\tilde{\mathbf{s}}_i[1 + \tilde{\mathbf{s}}_i'(\tilde{\mathbf{s}}_j\tilde{\mathbf{s}}_j' + \mathbf{I}_3)^{-1}\tilde{\mathbf{s}}_i]^{-1}\tilde{\mathbf{s}}_i'(\tilde{\mathbf{s}}_j\tilde{\mathbf{s}}_j' + \mathbf{I}_3)^{-1}.
\end{aligned}$$

Let $\mathbf{B} := (\tilde{\mathbf{s}}_j\tilde{\mathbf{s}}_j' + \mathbf{I}_3)^{-1}$, and so

$$(\Sigma(\mathbf{s}_i) + \Sigma(\mathbf{s}_j))^{-1} = \mathbf{B} - \mathbf{B}\tilde{\mathbf{s}}_i(1 + \tilde{\mathbf{s}}_i'\mathbf{B}\tilde{\mathbf{s}}_i)^{-1}\tilde{\mathbf{s}}_i'\mathbf{B} = \mathbf{B} - \frac{\mathbf{B}\tilde{\mathbf{s}}_i\tilde{\mathbf{s}}_i'\mathbf{B}}{1 + \tilde{\mathbf{s}}_i'\mathbf{B}\tilde{\mathbf{s}}_i},$$

$$\begin{aligned}
q^2(\mathbf{s}_i, \mathbf{s}_j) &\propto (\tilde{\mathbf{s}}_i - \tilde{\mathbf{s}}_j)'(\Sigma(\mathbf{s}_i) + \Sigma(\mathbf{s}_j))^{-1}(\tilde{\mathbf{s}}_i - \tilde{\mathbf{s}}_j) \\
&\propto (\tilde{\mathbf{s}}_i - \tilde{\mathbf{s}}_j)'\mathbf{B}(\tilde{\mathbf{s}}_i - \tilde{\mathbf{s}}_j) - \frac{1}{1 + \tilde{\mathbf{s}}_i'\mathbf{B}\tilde{\mathbf{s}}_i}(\tilde{\mathbf{s}}_i - \tilde{\mathbf{s}}_j)'\mathbf{B}\tilde{\mathbf{s}}_i\tilde{\mathbf{s}}_i'\mathbf{B}(\tilde{\mathbf{s}}_i - \tilde{\mathbf{s}}_j).
\end{aligned}$$

So computation of $q(\mathbf{s}_i, \mathbf{s}_j)$ only involves terms $\tilde{\mathbf{s}}_i'\mathbf{B}\tilde{\mathbf{s}}_i$, $\tilde{\mathbf{s}}_j'\mathbf{B}\tilde{\mathbf{s}}_j$ and $\tilde{\mathbf{s}}_i'\mathbf{B}\tilde{\mathbf{s}}_j$. Because

$$\mathbf{B} = (\tilde{\mathbf{s}}_j\tilde{\mathbf{s}}_j' + \mathbf{I}_3)^{-1} = \mathbf{I}_3 - \tilde{\mathbf{s}}_j(1 + \tilde{\mathbf{s}}_j'\tilde{\mathbf{s}}_j)^{-1}\tilde{\mathbf{s}}_j' = \mathbf{I}_3 - \frac{1}{2}\tilde{\mathbf{s}}_j\tilde{\mathbf{s}}_j',$$

we have

$$\begin{aligned}
\tilde{\mathbf{s}}_i'\mathbf{B}\tilde{\mathbf{s}}_i &= \tilde{\mathbf{s}}_i'\tilde{\mathbf{s}}_i - \frac{1}{2}(\tilde{\mathbf{s}}_i'\tilde{\mathbf{s}}_i)^2 = 1 - \frac{1}{2}(\tilde{\mathbf{s}}_i'\tilde{\mathbf{s}}_i)^2 \\
\tilde{\mathbf{s}}_j'\mathbf{B}\tilde{\mathbf{s}}_j &= \tilde{\mathbf{s}}_j'\tilde{\mathbf{s}}_j - \frac{1}{2}(\tilde{\mathbf{s}}_j'\tilde{\mathbf{s}}_j)^2 = 1 - \frac{1}{2} = \frac{1}{2} \\
\tilde{\mathbf{s}}_i'\mathbf{B}\tilde{\mathbf{s}}_j &= \tilde{\mathbf{s}}_i'\tilde{\mathbf{s}}_j - \frac{1}{2}(\tilde{\mathbf{s}}_i'\tilde{\mathbf{s}}_j)(\tilde{\mathbf{s}}_j'\tilde{\mathbf{s}}_j) = \tilde{\mathbf{s}}_i'\tilde{\mathbf{s}}_j - \frac{1}{2}\tilde{\mathbf{s}}_i'\tilde{\mathbf{s}}_j = \frac{1}{2}\tilde{\mathbf{s}}_i'\tilde{\mathbf{s}}_j.
\end{aligned}$$

Further,

$$\tilde{\mathbf{s}}_i'\tilde{\mathbf{s}}_j = [(\tilde{\mathbf{s}}_i - \tilde{\mathbf{s}}_j)'(\tilde{\mathbf{s}}_i - \tilde{\mathbf{s}}_j) - \tilde{\mathbf{s}}_i'\tilde{\mathbf{s}}_i - \tilde{\mathbf{s}}_j'\tilde{\mathbf{s}}_j] / 2 = [(\tilde{\mathbf{s}}_i - \tilde{\mathbf{s}}_j)'(\tilde{\mathbf{s}}_i - \tilde{\mathbf{s}}_j) - 2] / 2.$$

So $q(\mathbf{s}_i, \mathbf{s}_j)$ just depends on the distance $(\tilde{\mathbf{s}}_i - \tilde{\mathbf{s}}_j)'(\tilde{\mathbf{s}}_i - \tilde{\mathbf{s}}_j)$. For the normalization term $c(\mathbf{s}_i, \mathbf{s}_j)$, since we have proved that $|\boldsymbol{\Sigma}(\mathbf{s}_i)| = |\boldsymbol{\Sigma}(\mathbf{s}_j)| \equiv \gamma^2$,

$$\begin{aligned}
c(\mathbf{s}_i, \mathbf{s}_j) &= |\boldsymbol{\Sigma}(\mathbf{s}_i)|^{1/4} |\boldsymbol{\Sigma}(\mathbf{s}_j)|^{1/4} |(\boldsymbol{\Sigma}(\mathbf{s}_i) + \boldsymbol{\Sigma}(\mathbf{s}_j))/2|^{-1/2} \\
&\propto |(\boldsymbol{\Sigma}(\mathbf{s}_i) + \boldsymbol{\Sigma}(\mathbf{s}_j))^{-1}|^{1/2} \\
&\propto (|(\boldsymbol{\Sigma}(\mathbf{s}_i) + \boldsymbol{\Sigma}(\mathbf{s}_j))^{-1}| \cdot |(\tilde{\mathbf{s}}_i - \tilde{\mathbf{s}}_j)'(\tilde{\mathbf{s}}_i - \tilde{\mathbf{s}}_j)| / [(\tilde{\mathbf{s}}_i - \tilde{\mathbf{s}}_j)'(\tilde{\mathbf{s}}_i - \tilde{\mathbf{s}}_j)])^{1/2} \\
&\propto (|(\boldsymbol{\Sigma}(\mathbf{s}_i) + \boldsymbol{\Sigma}(\mathbf{s}_j))^{-1}| \cdot \det\{(\tilde{\mathbf{s}}_i - \tilde{\mathbf{s}}_j)(\tilde{\mathbf{s}}_i - \tilde{\mathbf{s}}_j)'\} / [(\tilde{\mathbf{s}}_i - \tilde{\mathbf{s}}_j)'(\tilde{\mathbf{s}}_i - \tilde{\mathbf{s}}_j)])^{1/2} \\
&\propto (\det\{(\boldsymbol{\Sigma}(\mathbf{s}_i) + \boldsymbol{\Sigma}(\mathbf{s}_j))^{-1}(\tilde{\mathbf{s}}_i - \tilde{\mathbf{s}}_j)(\tilde{\mathbf{s}}_i - \tilde{\mathbf{s}}_j)'\} / [(\tilde{\mathbf{s}}_i - \tilde{\mathbf{s}}_j)'(\tilde{\mathbf{s}}_i - \tilde{\mathbf{s}}_j)])^{1/2} \\
&\propto (\det\{(\tilde{\mathbf{s}}_i - \tilde{\mathbf{s}}_j)'(\boldsymbol{\Sigma}(\mathbf{s}_i) + \boldsymbol{\Sigma}(\mathbf{s}_j))^{-1}(\tilde{\mathbf{s}}_i - \tilde{\mathbf{s}}_j)\} / [(\tilde{\mathbf{s}}_i - \tilde{\mathbf{s}}_j)'(\tilde{\mathbf{s}}_i - \tilde{\mathbf{s}}_j)])^{1/2} \\
&\propto \left\{ \frac{q^2(\mathbf{s}_i, \mathbf{s}_j)}{(\tilde{\mathbf{s}}_i - \tilde{\mathbf{s}}_j)'(\tilde{\mathbf{s}}_i - \tilde{\mathbf{s}}_j)} \right\}^{1/2}.
\end{aligned} \tag{10}$$

We have proved that $q(\mathbf{s}_i, \mathbf{s}_j)$ just depends on $(\tilde{\mathbf{s}}_i - \tilde{\mathbf{s}}_j)'(\tilde{\mathbf{s}}_i - \tilde{\mathbf{s}}_j)$, so $c(\mathbf{s}_i, \mathbf{s}_j)$ also only depends on the distance $(\tilde{\mathbf{s}}_i - \tilde{\mathbf{s}}_j)'(\tilde{\mathbf{s}}_i - \tilde{\mathbf{s}}_j)$.

Overall, we can show

$$\rho_{NS}(\mathbf{s}_i, \mathbf{s}_j) = c(\mathbf{s}_i, \mathbf{s}_j) \rho(q(\mathbf{s}_i, \mathbf{s}_j))$$

only depends on the distance $(\tilde{\mathbf{s}}_i - \tilde{\mathbf{s}}_j)'(\tilde{\mathbf{s}}_i - \tilde{\mathbf{s}}_j)$, where $\rho(q)$ is a valid isotropic correlation function. So $\rho_{NS}(\mathbf{s}_i, \mathbf{s}_j)$ is isotropic. \square

Proof of Theorem 2. If $\kappa(\mathbf{s}) \equiv 0$ and $\gamma_1(\cdot), \gamma_2(\cdot)$ depend on L only, then $\mathcal{R}_x(\kappa(\mathbf{s})) \equiv \mathcal{R}_x(0) = \mathbf{I}_3$. Then

$$\tilde{\boldsymbol{\Sigma}}(\mathbf{s}) = \mathbf{D}(\gamma(\mathbf{s})) = \begin{pmatrix} 1 & 0 & 0 \\ 0 & \gamma_1(L) & 0 \\ 0 & 0 & \gamma_2(L) \end{pmatrix} = \begin{pmatrix} 1 & 0 & 0 \\ 0 & \gamma_1(L) & 0 \\ 0 & 0 & \gamma_1(L) \end{pmatrix} + \begin{pmatrix} 0 & 0 & 0 \\ 0 & 0 & 0 \\ 0 & 0 & \gamma_2(L) - \gamma_1(L) \end{pmatrix}.$$

Due to the results in Theorem 1, we have

$$\boldsymbol{\Sigma}(\mathbf{s}) = \mathcal{R}_z(l) \mathcal{R}_y(L) \tilde{\boldsymbol{\Sigma}}(\mathbf{s}) \mathcal{R}_y(L)' \mathcal{R}_z(l)' = (1 - \gamma_1(L)) \tilde{\mathbf{s}} \tilde{\mathbf{s}}' + \gamma_1(L) \mathbf{I}_3 + (\gamma_2(L) - \gamma_1(L)) \tilde{\mathbf{s}}^* (\tilde{\mathbf{s}}^*)',$$

where

$$\tilde{\mathbf{s}}^* = \begin{pmatrix} \cos(l) \sin(L) \\ \sin(l) \sin(L) \\ \cos(L) \end{pmatrix}, \quad (\tilde{\mathbf{s}}^*)'(\tilde{\mathbf{s}}^*) = 1.$$

Thus

$$\begin{aligned}
|\boldsymbol{\Sigma}(\mathbf{s})| &= \det\{(1 - \gamma_1(L)) \tilde{\mathbf{s}} \tilde{\mathbf{s}}' + \gamma_1(L) \mathbf{I}_3 + (\gamma_2(L) - \gamma_1(L)) \tilde{\mathbf{s}}^* (\tilde{\mathbf{s}}^*)'\} \\
&= \gamma_1(L)^3 \cdot \det\left\{ \frac{1 - \gamma_1(L)}{\gamma_1(L)} \tilde{\mathbf{s}} \tilde{\mathbf{s}}' + \frac{\gamma_2(L) - \gamma_1(L)}{\gamma_1(L)} \tilde{\mathbf{s}}^* (\tilde{\mathbf{s}}^*)' + \mathbf{I}_3 \right\} \\
&= \gamma_1(L)^3 \cdot \det\left\{ \begin{pmatrix} \frac{1 - \gamma_1(L)}{\gamma_1(L)} \tilde{\mathbf{s}} & \frac{\gamma_2(L) - \gamma_1(L)}{\gamma_1(L)} \tilde{\mathbf{s}}^* \end{pmatrix} \begin{pmatrix} \tilde{\mathbf{s}}' \\ (\tilde{\mathbf{s}}^*)' \end{pmatrix} + \mathbf{I}_3 \right\} \\
&= \gamma_1(L)^3 \cdot \det\left\{ \begin{pmatrix} \tilde{\mathbf{s}}' \\ (\tilde{\mathbf{s}}^*)' \end{pmatrix} \begin{pmatrix} \frac{1 - \gamma_1(L)}{\gamma_1(L)} \tilde{\mathbf{s}} & \frac{\gamma_2(L) - \gamma_1(L)}{\gamma_1(L)} \tilde{\mathbf{s}}^* \end{pmatrix} + \mathbf{I}_2 \right\} \\
&= \gamma_1(L)^3 \cdot \begin{vmatrix} \frac{1 - \gamma_1(L)}{\gamma_1(L)} + 1 & 2 \sin(L) \cos(L) \\ 2 \sin(L) \cos(L) & \frac{\gamma_2(L) - \gamma_1(L)}{\gamma_1(L)} + 1 \end{vmatrix} \\
&= \gamma_1(L) \gamma_2(L) - 4 \gamma_1(L)^3 \sin^2(L) \cos^2(L)
\end{aligned}$$

only depend on L . WLOG, ignore $\gamma_1(L)$, $\gamma_2(L)$ again (they only depend on L),

$$\begin{aligned}
(\boldsymbol{\Sigma}(\mathbf{s}_i) + \boldsymbol{\Sigma}(\mathbf{s}_j))^{-1} &= [\tilde{\mathbf{s}}_i \tilde{\mathbf{s}}_i' + \tilde{\mathbf{s}}_i^* (\tilde{\mathbf{s}}_i^*)' + \tilde{\mathbf{s}}_j \tilde{\mathbf{s}}_j' + \tilde{\mathbf{s}}_j^* (\tilde{\mathbf{s}}_j^*)' + \mathbf{I}_3]^{-1} \\
&= \left[\begin{pmatrix} \tilde{\mathbf{s}}_i & \tilde{\mathbf{s}}_i^* \end{pmatrix} \begin{pmatrix} \tilde{\mathbf{s}}_i' \\ (\tilde{\mathbf{s}}_i^*)' \end{pmatrix} + \begin{pmatrix} \tilde{\mathbf{s}}_j & \tilde{\mathbf{s}}_j^* \end{pmatrix} \begin{pmatrix} \tilde{\mathbf{s}}_j' \\ (\tilde{\mathbf{s}}_j^*)' \end{pmatrix} + \mathbf{I}_3 \right]^{-1} \\
&= \mathbf{V}^{-1} - \mathbf{V}^{-1} \begin{pmatrix} \tilde{\mathbf{s}}_i & \tilde{\mathbf{s}}_i^* \end{pmatrix} \left[\mathbf{I}_2 + \begin{pmatrix} \tilde{\mathbf{s}}_i' \\ (\tilde{\mathbf{s}}_i^*)' \end{pmatrix} \mathbf{V}^{-1} \begin{pmatrix} \tilde{\mathbf{s}}_i & \tilde{\mathbf{s}}_i^* \end{pmatrix} \right]^{-1} \begin{pmatrix} \tilde{\mathbf{s}}_i' \\ (\tilde{\mathbf{s}}_i^*)' \end{pmatrix} \mathbf{V}^{-1} \\
&= \mathbf{V}^{-1} - \mathbf{V}^{-1} \begin{pmatrix} \tilde{\mathbf{s}}_i & \tilde{\mathbf{s}}_i^* \end{pmatrix} \left[\mathbf{I}_2 + \begin{pmatrix} \tilde{\mathbf{s}}_i' \mathbf{V}^{-1} \tilde{\mathbf{s}}_i & \tilde{\mathbf{s}}_i' \mathbf{V}^{-1} \tilde{\mathbf{s}}_i^* \\ (\tilde{\mathbf{s}}_i^*)' \mathbf{V}^{-1} \tilde{\mathbf{s}}_i & (\tilde{\mathbf{s}}_i^*)' \mathbf{V}^{-1} \tilde{\mathbf{s}}_i^* \end{pmatrix} \right]^{-1} \begin{pmatrix} \tilde{\mathbf{s}}_i' \\ (\tilde{\mathbf{s}}_i^*)' \end{pmatrix} \mathbf{V}^{-1},
\end{aligned}$$

where

$$\mathbf{V} = \begin{pmatrix} \tilde{\mathbf{s}}_j & \tilde{\mathbf{s}}_j^* \end{pmatrix} \begin{pmatrix} \tilde{\mathbf{s}}_j' \\ (\tilde{\mathbf{s}}_j^*)' \end{pmatrix} + \mathbf{I}_3.$$

Then

$$\begin{aligned}
q^2(\mathbf{s}_i, \mathbf{s}_j) &\propto (\tilde{\mathbf{s}}_i - \tilde{\mathbf{s}}_j)' (\boldsymbol{\Sigma}(\mathbf{s}_i) + \boldsymbol{\Sigma}(\mathbf{s}_j))^{-1} (\tilde{\mathbf{s}}_i - \tilde{\mathbf{s}}_j) \\
&\propto (\tilde{\mathbf{s}}_i - \tilde{\mathbf{s}}_j)' \mathbf{V}^{-1} (\tilde{\mathbf{s}}_i - \tilde{\mathbf{s}}_j) - (\tilde{\mathbf{s}}_i - \tilde{\mathbf{s}}_j)' \mathbf{V}^{-1} \begin{pmatrix} \tilde{\mathbf{s}}_i & \tilde{\mathbf{s}}_i^* \end{pmatrix} \left[\mathbf{I}_2 + \begin{pmatrix} \tilde{\mathbf{s}}_i' \mathbf{V}^{-1} \tilde{\mathbf{s}}_i & \tilde{\mathbf{s}}_i' \mathbf{V}^{-1} \tilde{\mathbf{s}}_i^* \\ (\tilde{\mathbf{s}}_i^*)' \mathbf{V}^{-1} \tilde{\mathbf{s}}_i & (\tilde{\mathbf{s}}_i^*)' \mathbf{V}^{-1} \tilde{\mathbf{s}}_i^* \end{pmatrix} \right]^{-1} \\
&\quad \begin{pmatrix} \tilde{\mathbf{s}}_i' \\ (\tilde{\mathbf{s}}_i^*)' \end{pmatrix} \mathbf{V}^{-1} (\tilde{\mathbf{s}}_i - \tilde{\mathbf{s}}_j).
\end{aligned}$$

Because

$$\begin{aligned}
\mathbf{V}^{-1} &= \mathbf{I}_3 - \begin{pmatrix} \tilde{\mathbf{s}}_j & \tilde{\mathbf{s}}_j^* \end{pmatrix} \left[\mathbf{I}_2 + \begin{pmatrix} 1 & \tilde{\mathbf{s}}_j' \tilde{\mathbf{s}}_j^* \\ (\tilde{\mathbf{s}}_j^*)' \tilde{\mathbf{s}}_j & 1 \end{pmatrix} \right]^{-1} \begin{pmatrix} \tilde{\mathbf{s}}_j' \\ (\tilde{\mathbf{s}}_j^*)' \end{pmatrix} \\
&= \mathbf{I}_3 - \frac{1}{4 - (\tilde{\mathbf{s}}_j' \tilde{\mathbf{s}}_j^*)^2} \begin{pmatrix} \tilde{\mathbf{s}}_j & \tilde{\mathbf{s}}_j^* \end{pmatrix} \left[\begin{pmatrix} 2 & -\tilde{\mathbf{s}}_j' \tilde{\mathbf{s}}_j^* \\ -(\tilde{\mathbf{s}}_j^*)' \tilde{\mathbf{s}}_j & 2 \end{pmatrix} \right]^{-1} \begin{pmatrix} \tilde{\mathbf{s}}_j' \\ (\tilde{\mathbf{s}}_j^*)' \end{pmatrix},
\end{aligned}$$

we can figure out that the computation of $q^2(\mathbf{s}_i, \mathbf{s}_j)$ only involves the following types of terms

$$\left\{ \begin{aligned}
&\tilde{\mathbf{s}}_i' \tilde{\mathbf{s}}_i = 1 \\
&\tilde{\mathbf{s}}_i' \tilde{\mathbf{s}}_i^* = \tilde{\mathbf{s}}_i' \cdot \left[(\tan(s_{i2})) \tilde{\mathbf{s}}_i + \left(0, 0, \cos(s_{i2}) - \frac{\sin^2(s_{i2})}{\cos(s_{i2})} \right)' \right] = \tan(s_{i2}) + \sin(s_{i2}) \left[\cos(s_{i2}) - \frac{\sin^2(s_{i2})}{\cos(s_{i2})} \right] \\
&(\tilde{\mathbf{s}}_i^*)' \tilde{\mathbf{s}}_i^* = 1 \\
&(\tilde{\mathbf{s}}_i^*)' \tilde{\mathbf{s}}_j^* = \left[(\tan(s_{i2})) \tilde{\mathbf{s}}_i + \left(0, 0, \cos(s_{i2}) - \frac{\sin^2(s_{i2})}{\cos(s_{i2})} \right)' \right]' \cdot \left[(\tan(s_{j2})) \tilde{\mathbf{s}}_j + \left(0, 0, \cos(s_{j2}) - \frac{\sin^2(s_{j2})}{\cos(s_{j2})} \right)' \right] \\
&\quad = \tan(s_{i2}) \tan(s_{j2}) (\tilde{\mathbf{s}}_i' \tilde{\mathbf{s}}_j) + \tan(s_{i2}) \sin(s_{i2}) \left[\cos(s_{j2}) - \frac{\sin^2(s_{j2})}{\cos(s_{j2})} \right] \\
&\quad \quad + \tan(s_{j2}) \sin(s_{j2}) \left[\cos(s_{i2}) - \frac{\sin^2(s_{i2})}{\cos(s_{i2})} \right] + \left[\cos(s_{i2}) - \frac{\sin^2(s_{i2})}{\cos(s_{i2})} \right] \left[\cos(s_{j2}) - \frac{\sin^2(s_{j2})}{\cos(s_{j2})} \right] \\
&\tilde{\mathbf{s}}_i' \tilde{\mathbf{s}}_j^* = \tan(s_{j2}) (\tilde{\mathbf{s}}_i' \tilde{\mathbf{s}}_j) + \sin(s_{i2}) \left[\cos(s_{j2}) - \frac{\sin^2(s_{j2})}{\cos(s_{j2})} \right] \\
&\tilde{\mathbf{s}}_j' \tilde{\mathbf{s}}_i^* = \tan(s_{i2}) (\tilde{\mathbf{s}}_j' \tilde{\mathbf{s}}_i) + \sin(s_{j2}) \left[\cos(s_{i2}) - \frac{\sin^2(s_{i2})}{\cos(s_{i2})} \right] \\
&\tilde{\mathbf{s}}_i' \tilde{\mathbf{s}}_j = [(\tilde{\mathbf{s}}_i - \tilde{\mathbf{s}}_j)' (\tilde{\mathbf{s}}_i - \tilde{\mathbf{s}}_j) - 2] / 2.
\end{aligned} \right.$$

We can change the index i to j for the first 3 terms and they are still valid. Thus these values only depend on s_{i2} , s_{j2} and $\tilde{\mathbf{s}}_i' \tilde{\mathbf{s}}_j$, and $\tilde{\mathbf{s}}_i' \tilde{\mathbf{s}}_j$ can be expressed in terms of the distance $(\tilde{\mathbf{s}}_i - \tilde{\mathbf{s}}_j)' (\tilde{\mathbf{s}}_i - \tilde{\mathbf{s}}_j)$. The computation of $q^2(\mathbf{s}_i, \mathbf{s}_j)$ only depends on the distance $(\tilde{\mathbf{s}}_i - \tilde{\mathbf{s}}_j)' (\tilde{\mathbf{s}}_i - \tilde{\mathbf{s}}_j)$ and the longitudes s_{i2} , s_{j2} . Similar to (10) in the proof of Theorem 1, we can also show that $c(\mathbf{s}_i, \mathbf{s}_j)$ is a function of $(\tilde{\mathbf{s}}_i - \tilde{\mathbf{s}}_j)' (\tilde{\mathbf{s}}_i - \tilde{\mathbf{s}}_j)$, s_{i2} and s_{j2} . Then $\rho_{NS}(\mathbf{s}_i, \mathbf{s}_j) = c(\mathbf{s}_i, \mathbf{s}_j) \rho(q(\mathbf{s}_i, \mathbf{s}_j)) := \rho_A(\tilde{\mathbf{s}}_i - \tilde{\mathbf{s}}_j, s_{i2}, s_{j2})$, so it is axially symmetric. \square

References

- Alegría, A., Cuevas-Pacheco, F., Diggle, P., and Porcu, E. (2021). The f-family of covariance functions: A matérn analogue for modeling random fields on spheres. *Spatial Statistics*, 43:100512.
- Banerjee, S., Gelfand, A. E., Finley, A. O., and Sang, H. (2008). Gaussian predictive process models for large spatial data sets. *Journal of the Royal Statistical Society, Series B*, 70(4):825–848.
- Blake, L. R., Porcu, E., and Hammerling, D. M. (2022). Parametric nonstationary covariance functions on spheres. *Stat*, to appear.
- Castruccio, S. and Genton, M. G. (2014). Beyond axial symmetry: An improved class of models for global data. *Stat*, 3(1):48–55.
- Castruccio, S. and Genton, M. G. (2016). Compressing an ensemble with statistical models: An algorithm for global 3d spatio-temporal temperature. *Technometrics*, 58(3):319–328.
- Castruccio, S., Stein, M. L., et al. (2013). Global space–time models for climate ensembles. *The Annals of Applied Statistics*, 7(3):1593–1611.
- Du, J., Ma, C., and Li, Y. (2013). Isotropic variogram matrix functions on spheres. *Mathematical Geosciences*, 45(3):341–357.
- Emery, X., Arroyo, D., and Mery, N. (2021). Twenty-two families of multivariate covariance kernels on spheres, with their spectral representations and sufficient validity conditions. *Stochastic Environmental Research and Risk Assessment*, pages 1–21.
- Gneiting, T. (2013). Strictly and non-strictly positive definite functions on spheres. *Bernoulli*, 19(4):1327–1349.
- Guinness, J. (2018). Permutation and Grouping Methods for Sharpening Gaussian Process Approximations. *Technometrics*, 60(4):415–429.
- Guinness, J. and Fuentes, M. (2016). Isotropic covariance functions on spheres: Some properties and modeling considerations. *Journal of Multivariate Analysis*, 143:143–152.
- Heaton, M., Katzfuss, M., Berrett, C., and Nychka, D. (2014). Constructing valid spatial processes on the sphere using kernel convolutions. *Environmetrics*, 25(1):2–15.
- Hitczenko, M. and Stein, M. L. (2012). Some theory for anisotropic processes on the sphere. *Statistical Methodology*, 9(1-2):211–227.
- Huang, C., Zhang, H., and Robeson, S. M. (2011). On the validity of commonly used covariance and variogram functions on the sphere. *Mathematical Geosciences*, 43(6):721–733.
- Jeong, J., Jun, M., and Genton, M. G. (2017). Spherical process models for global spatial statistics. *Statistical Science*, 32(4):501.
- Jones, R. (1963). Stochastic processes on a sphere. *Annals of Mathematical Statistics*, 34(1):213–218.
- Jun, M. (2014). Matérn-based nonstationary cross-covariance models for global processes. *Journal of Multivariate Analysis*, 128:134–146.
- Jun, M. and Stein, M. L. (2007). An approach to producing space–time covariance functions on spheres. *Technometrics*, 49(4):468–479.
- Jun, M. and Stein, M. L. (2008). Nonstationary covariance models for global data. *Annals of Applied Statistics*, 2(4):1271–1289.
- Kang, M. and Katzfuss, M. (2021). Correlation-based sparse inverse Cholesky factorization for fast Gaussian-process inference. *arXiv:2112.14591*.
- Katzfuss, M. (2011). *Hierarchical Spatial and Spatio-Temporal Modeling of Massive Datasets, with Application to Global Mapping of CO₂*. PhD thesis, The Ohio State University.
- Katzfuss, M. and Guinness, J. (2021). A general framework for Vecchia approximations of Gaussian processes. *Statistical Science*, 36(1):124–141.
- Katzfuss, M., Guinness, J., Gong, W., and Zilber, D. (2020a). Vecchia approximations of Gaussian-process predictions. *Journal of Agricultural, Biological, and Environmental Statistics*, 25(3):383–414.
- Katzfuss, M., Guinness, J., and Lawrence, E. (2022). Scaled Vecchia approximation for fast computer-model emulation. *SIAM/ASA Journal on Uncertainty Quantification*, 10(2):537–554.

- Katzfuss, M., Jurek, M., Zilber, D., Gong, W., Guinness, J., Zhang, J., and Schäfer, F. (2020b). *GPvecchia: Fast Gaussian-process inference using Vecchia approximations*. R package version 0.1.3.
- Kay, J. E., Deser, C., Phillips, A., Mai, A., Hannay, C., Strand, G., Arblaster, J. M., Bates, S. C., Danabasoglu, G., Edwards, J., Holland, M., Kushner, P., Lamarque, J. F., Lawrence, D., Lindsay, K., Middleton, A., Munoz, E., Neale, R., Oleson, K., Polvani, L., and Vertenstein, M. (2015). The Community Earth System Model (CESM) Large Ensemble Project: A community resource for studying climate change in the presence of internal climate variability. *Bulletin of the American Meteorological Society*, 96(8):1333–1349.
- Knapp, A. (2012). Global Bayesian Nonstationary Spatial Modeling For Very Large Datasets. *Bachelor Thesis*.
- Lindgren, F., Rue, H., and Lindström, J. (2011). An explicit link between gaussian fields and gaussian markov random fields: the stochastic partial differential equation approach. *Journal of the Royal Statistical Society: Series B (Statistical Methodology)*, 73(4):423–498.
- Ma, C. (2012). Stationary and isotropic vector random fields on spheres. *Mathematical Geosciences*, 44(6):765–778.
- Ma, C. (2015). Isotropic covariance matrix functions on all spheres. *Mathematical Geosciences*, 47(6):699–717.
- Menegatto, V. (2020). Positive definite functions on products of metric spaces via generalized stieltjes functions. *Proceedings of the American Mathematical Society*, 148(11):4781–4795.
- Paciorek, C. and Schervish, M. (2006). Spatial modelling using a new class of nonstationary covariance functions. *Environmetrics*, 17(5):483–506.
- Schäfer, F., Katzfuss, M., and Owhadi, H. (2021). Sparse Cholesky factorization by Kullback-Leibler minimization. *SIAM Journal on Scientific Computing*, 43(3):A2019–A2046.
- Stein, M. L. (2005). Nonstationary spatial covariance functions. *Technical Report No. 21, University of Chicago*.
- Stein, M. L. et al. (2007). Spatial variation of total column ozone on a global scale. *The Annals of Applied Statistics*, 1(1):191–210.
- Vecchia, A. (1988). Estimation and model identification for continuous spatial processes. *Journal of the Royal Statistical Society, Series B*, 50(2):297–312.
- Vihola, M. (2012). Robust adaptive metropolis algorithm with coerced acceptance rate. *Statistics and Computing*, 22(5):997–1008.
- Yaglom, A. (1987). *Correlation Theory of Stationary and Related Random Functions, Vol. 1*. Springer, New York, NY.